# Lateral Superlattice - A Possible Origin of the Large Leakage Current in $Al_{1-x}Sc_xN$

Wanwang Yang, Chenxi Yu, Fei Liu†, Jinfeng Kang‡
School of Integrated Circuits, Peking University, Beijing 100871, China
E-mails: †feiliu@pku.edu.cn, ‡kangjf@pku.edu.cn

***Abstract*—In this work, the Sc doping effect on the structure and ferroelectric properties of $Al_{1-x}Sc_xN$ are investigated based on density functional theory calculations combined with a structure prediction evolutionary algorithm. It is found that as the Sc concentration increases, a stable phase with the lateral superlattice (SL) emerges in $Al_{1-x}Sc_xN$, in which wurtzite (WZ) AlN and rocksalt (RS) ScN are alternating along the WZ-[10$\bar{1}$0] direction. The rapid decline of band gap in lateral-SL $Al_{1-x}Sc_xN$ with increasing Sc concentration is induced by the RS-ScN part. As shown in the local density of states map, the RS-ScN part has a prominently smaller band gap than the wurtzite AlN part, and corresponding high electric conductivity. It means the RS-ScN part would act as a dominant channel of leakage current in the lateral-SL $Al_{1-x}Sc_xN$. These results suggest one of the possible causes responsible for the leakage current paths in $Al_{1-x}Sc_xN$ thin films.**

***Keywords—$Al_{1-x}Sc_xN$, lateral superlattice, leakage, DFT***

## I. Introduction

Since the discovery of the tremendous enhancement of piezoelectric response in Sc-doped wurtzite $Al_{1-x}Sc_xN$ films [1], the $Al_{1-x}Sc_xN$-based piezoelectric devices have attracted much research attention. Recently, $Al_{1-x}Sc_xN$ thin films have been demonstrated to be ferroelectric with large polarization and high Curie temperature, presenting promising materials for multi-functional devices which could integrate the ferroelectric memory function into III-nitride-based piezoelectric devices [2-4]. However, the unexpectedly large leakage current, leading to higher power consumption, worse reliability, and limited ability of scaling down, hinders practical integration and efficient applications. Though previous studies have revealed that leakage current is closely related to defects in $Al_{1-x}Sc_xN$ [4-6], the origin of the large leakage is still under debate. Meanwhile, there is a phase transition in $Al_{1-x}Sc_xN$ as Sc concentration increases, due to the different stable structures of AlN (wurtzite, WZ) and ScN (rocksalt, RS) shown in Figs. 1(a-b). The intermediate phase structure and phase boundary are unclear, and need further studies [7,8].

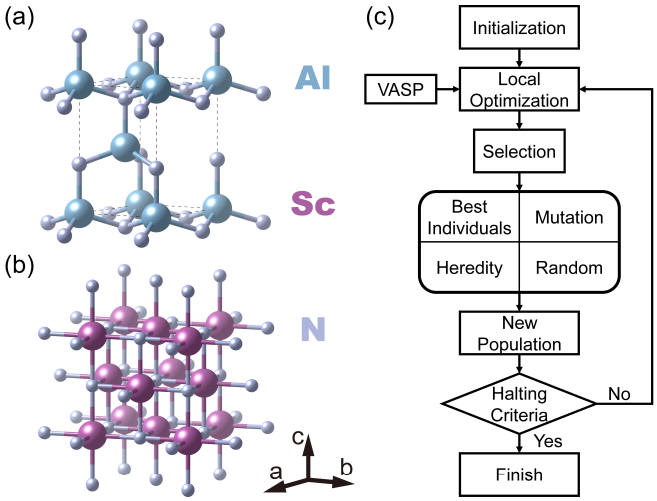


Fig. 1. Crystal structures of (a) WZ-AlN and (b) RS-ScN. (c) Flowchart of the evolutionary algorithm implemented in USPEX.

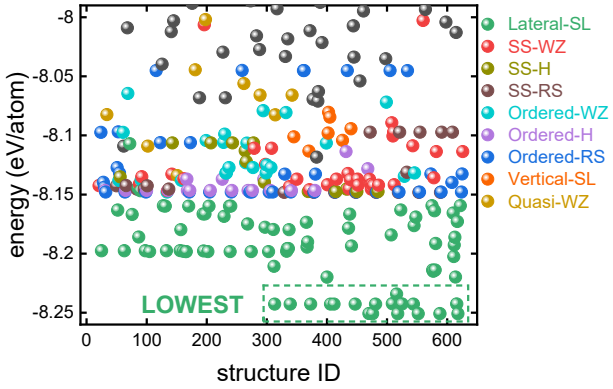


Fig. 2. Energy of various structures of $Al_{0.5}Sc_{0.5}N$ with 32 atoms in the unit cell, generated by the evolutionary algorithm. It shows clearly that the lateral-SL has the lowest energy, considered as the most stable structure.

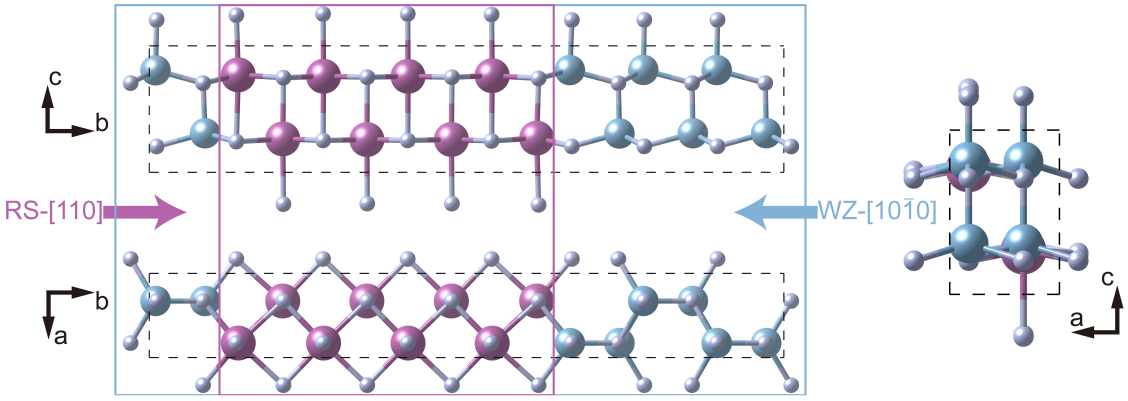


Fig. 3. Top and side views of the lateral-SL $Al_{0.5}Sc_{0.5}N$ crystal structure, which is the predicted most stable structure. This lateral-SL is constructed by a WZ-AlN part and a RS-ScN part, along the WZ-[10$\bar{1}$0] direction, parallel with the RS-[110] direction.

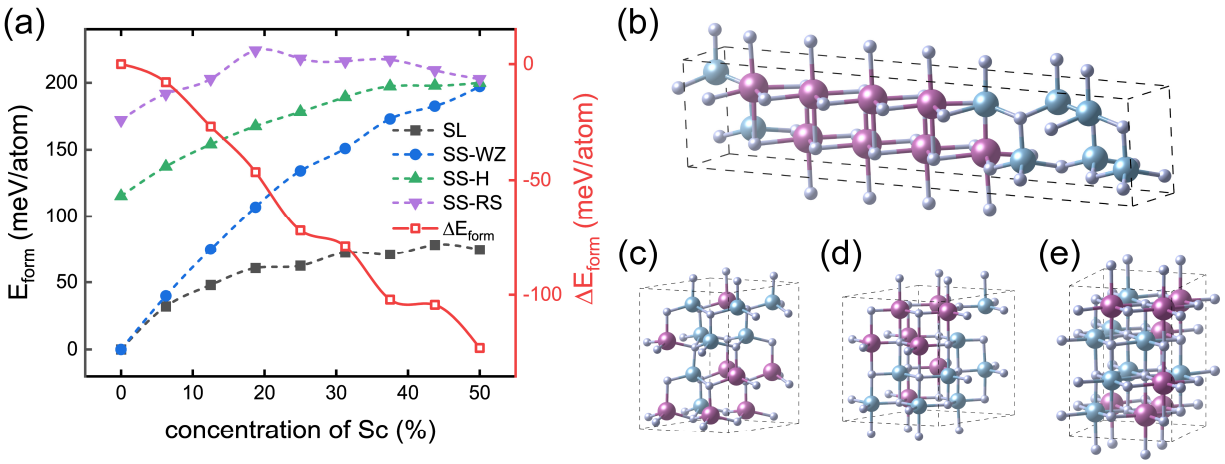


Fig. 4. (a) The formation energy of 4 phases $Al_{1-x}Sc_xN$ as functions of Sc concentration (left axis); The difference in the formation energy between SL and SS-WZ (right axis). Crystal structures of (b) SL, (c) SS-WZ, (d) SS-H, and (e) SS-RS $Al_{0.5}Sc_{0.5}N$.

In this study, we investigated the impact of Sc doping effect on the structure of $Al_{1-x}Sc_xN$ to comprehend its leakage behavior and ferroelectric properties, based on density functional theory (DFT) calculations combined with a structure prediction evolutionary algorithm. A new phase, named as lateral superlattice (SL) here, consisting of WZ-AlN and RS-ScN, is found to be the most stable structure for Sc-doped $Al_{1-x}Sc_xN$. The WZ-AlN part of lateral-SL works as a resolute polar unit, while the RS-ScN part shows weaker polar as Sc concentration increases. Additionally, local density of states (LDOS) analysis shows that the RS-ScN part presents a much smaller band gap than the WZ-AlN part, resulting in high conductivity. Such a result suggests that the RS-ScN part in the SL structure could act as a dominant leakage current channel. The presented structure model, lateral-SL $Al_{1-x}Sc_xN$, could well explain the leakage behavior of Sc-alloyed $Al_{1-x}Sc_xN$ with increasing Sc concentration.

## II. Simulation Method

An evolutionary algorithm in USPEX code [9-11], illustrated by Fig. 1(c), is implemented to predict the thermodynamically stable structures of $Al_{1-x}Sc_xN$ with 32-atom cells. The Sc doping concentration varies from 0 to 50% at 6.25% intervals. The special quasirandom structures (SQSs) are constructed to mimic the disordered SS WZ, layered-hexagonal (H), and RS $Al_{1-x}Sc_xN$ [12].

All DFT calculations presented in this work were performed with the PBE exchange-correlation functionals and the PAW pseudo-potentials implemented in the VASP code [13-16]. The numbers of valence electrons for Al, Sc, and N were set to 3, 11, and 5, respectively. The spontaneous polarization was calculated using the Berry phase approach with the reference H phase [17-19]. The polarization switching barriers were calculated using the solid-state nudged elastic band (SS-NEB) method [20], which allows the relaxation of both atomic positions and lattice vectors. The LDOS map was obtained with DensityTool [21], a post-program to VASP. All crystal models in this work were visualized by the Visualization for Electronic and STructural Analysis (VESTA) program [22].

## III. Results and Discussion

The result of the structure prediction evolutionary algorithm in $Al_{0.5}Sc_{0.5}N$ with 32-atoms cell is depicted in Fig. 2. Various ordered and disordered structures are generated by this evolutionary algorithm. It shows clearly that the most stable structure, with the lowest energy, is the lateral-SL after the halting criteria are achieved. This novel lateral-SL consists of two kinds of phases, WZ-AlN and RS-ScN, and the phase interface is perpendicular to the WZ-$[10\bar{1}0]$ direction and RS-[110] direction, as illustrated by Fig. 3. In the lateral-SL, each Al atom and Sc atom have 4 and 6 nearest neighbor N atoms, respectively, which means all atoms possess a similar local bond structure to that of the stable WZ-AlN and RS-ScN, except the atoms near the phase interface that are affected slightly by the difference in N-Al-N and N-Sc-N bond angles.

The formation energy of the lateral-SL, SS-WZ, SS-H, and SS-RS is calculated as functions of Sc concentration shown in Fig. 4(a), given by:

$$E_{form} = E_{AlScN} - (1 - c(Sc))E_{AlN}^{WZ} - c(Sc)E_{ScN}^{RS}. \quad (1)$$

The difference between SL and SS-WZ formation energy is depicted by the red solid line to the left axis, which gets larger as the Sc concentration increases. This result is expected from the stable local bond structure of lateral-SL mentioned above. It suggests that the lateral-SL is more likely to appear in $Al_{1-x}Sc_xN$ with higher Sc concentration.

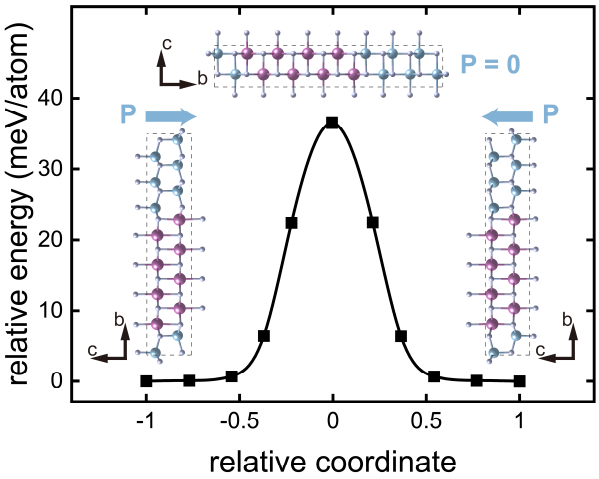


Fig. 5. Energy landscape of the lateral-SL $Al_{0.5}Sc_{0.5}N$ along the switching path. Insets present the initial (Al-polar, polarization down), transition, and final (N-polar, polarization down) states of the lateral-SL

The lateral-SL $Al_{1-x}Sc_xN$ is a polar structure due to the polar WZ-AlN part. Fig. 5 describes the switching path of the lateral-SL $Al_{0.5}Sc_{0.5}N$, along which the WZ-AlN part switches from the Al-polar state to the N-polar state while the RS-ScN part barely moved. The switching barriers and polarization between lateral-SL and SS-WZ with different Sc doping concentrations are compared in Figs. 6(a-b). These figures show that switching barriers and polarization decrease with incremental Sc concentrations in both lateral-SL and SS-WZ, consistent with previous works [2,4,8]. Only the polarization of the lateral-SL deviates from a nearly linear decreasing trend, shown clearly in Fig. 6(b) with the aid of the linear combination polarization. This result arises from the much more rapid increase of WZ internal parameter u in lateral-SL, compared with SS-WZ, illustrated by Fig. 7.

Fig. 8 shows band gaps of the lateral-SL, SS-WZ, SS-H, and SS-RS as functions of the Sc concentration. The band gaps of SS-WZ and SS-H decrease nearly linearly with incremental Sc concentration, whereas those of lateral-SL and SS-RS decrease similarly and more rapidly. These results indicate that the band gap of lateral-SL is mainly affected by the RS-ScN part, which has the same crystal structure with SS-RS. LDOS analysis confirms that the decreasing behavior of the band gap in lateral-SL is dominated by the RS-ScN part, which has a much narrower band gap compared with the WZ-AlN part, as shown in Fig. 9. Consequently, the RS-ScN part has higher electric conductivity and could act as a dominant channel of leakage current in lateral-SL, which could be a possible origin of the large leakage current in $Al_{1-x}Sc_xN$ thin films with high Sc concentration.

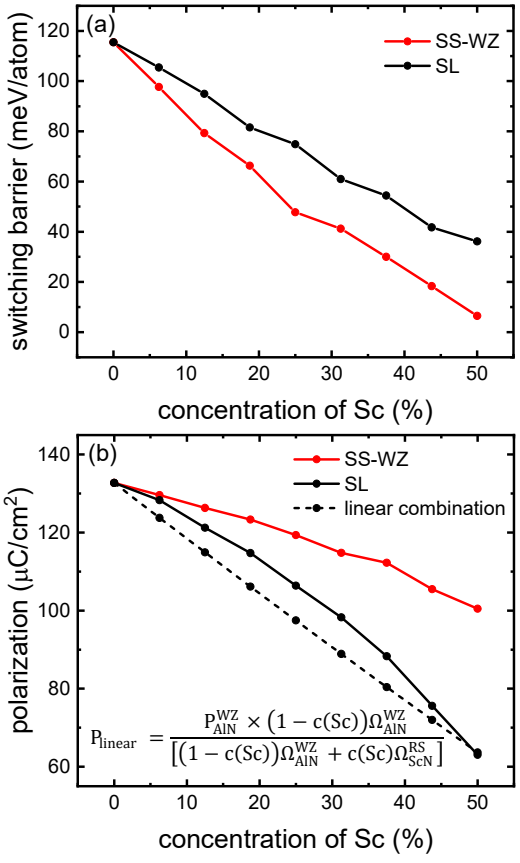


Fig. 6. (a) Switching barriers of SS-WZ and lateral-SL $Al_{1-x}Sc_xN$ as functions of Sc concentration. (b) Polarization of SS-WZ and lateral-SL $Al_{1-x}Sc_xN$ as functions of Sc concentration. The dashed line shows the polarization calculated by the inserted linear function.

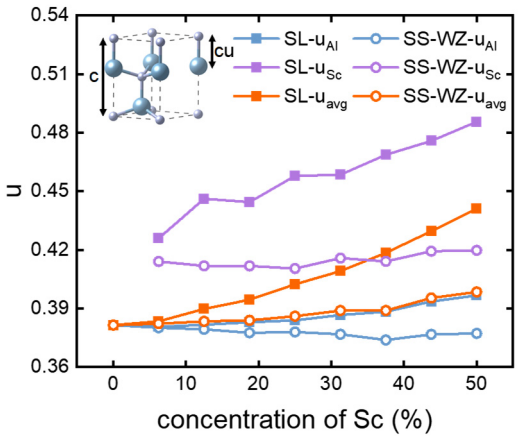


Fig. 7. The averaged WZ internal parameter u of lateral-SL (solid square) and SS-WZ (open circle) $Al_{1-x}Sc_xN$ as functions of Sc concentration. The dashed lines present the Al and Sc site resolved values, while the solid lines are the compositional weighted values. The inset illustrates the WZ internal parameter u in WZ-AlN.

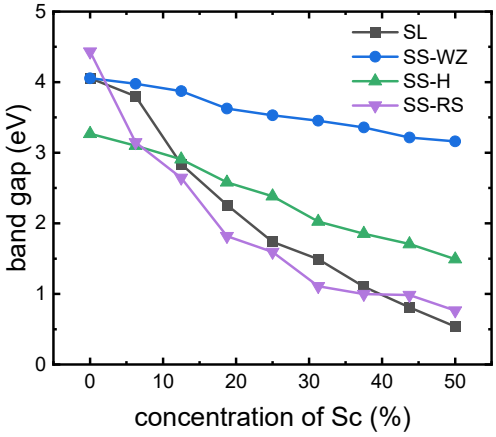


Fig. 8. Band gaps of 4 phases $Al_{1-x}Sc_xN$ as functions of Sc concentration. Band gaps of SS-WZ and SS-H decrease almost linearly with incremental Sc concentration, while those of lateral-SL and SS-RS decrease much more rapidly.

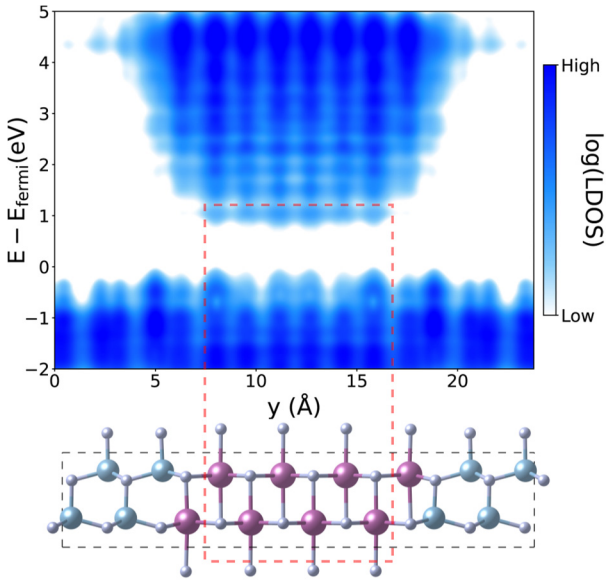


Fig. 9. LDOS heat map of lateral-SL $Al_{0.5}Sc_{0.5}N$ along the b axis (up panel) and the corresponding side view of lateral-SL $Al_{0.5}Sc_{0.5}N$ crystal structure. As the red dashed rectangle depicts, the RS-ScN part of lateral-SL has a much narrower band gap than the WZ-AlN part.

## IV. Conclusion

We studied the impacts of Sc doping concentration on the crystal structure and ferroelectric properties of $Al_{1-x}Sc_xN$, based on DFT calculations combined with a structure prediction evolutionary algorithm. A lateral-SL structure, consisting of a polar WZ-AlN part and an almost non-polar RS-ScN part, emerges as the stable phase of $Al_{1-x}Sc_xN$ with high Sc concentration. Comparable with SS-RS, the RS-ScN part possesses a much smaller band gap than the WZ-AlN part, which can result in the higher conduction current. This suggests that the RS-ScN part might act as a leakage channel in lateral-SL, and could induce a considerable leakage current. These findings provide valuable insights into the mechanism of leakage behavior in $Al_{1-x}Sc_xN$.

## Acknowledgment

This work was supported by National Key Research and Development Program (Grant No. 2019YFB2205100) and National Natural Science Foundation of China (Grant No. 92064001). Computational resources were provided by the High-performance Computing Platform of Peking University and the National SuperComputerCenter in Tianjin.

## References

[1] M. Akiyama, T. Kamohara, K. Kano, A. Teshigahara, Y. Takeuchi, and N. Kawahara, "Enhancement of Piezoelectric Response in Scandium Aluminum Nitride Alloy Thin Films Prepared by Dual Reactive Cosputtering," *Adv. Mater.,* vol. 21, no. 5, pp. 593-596, 2009.

[2] S. Fichtner, N. Wolff, F. Lofink, L. Kienle, and B. Wagner, "AlScN: A III-V semiconductor based ferroelectric," *Journal of Applied Physics,* vol. 125, no. 11, pp. 114103, 2019.

[3] J. Casamento, K. Nomoto, T. S. Nguyen, H. Lee, C. Savant, L. Li, A. Hickman, T. Maeda, J. Encomendero, V. Gund, A. Lal, J. C. M. Hwang, H. G. Xing, and D. Jena, "FerroHEMTs: High-Current and High-Speed All-Epitaxial AlScN/GaN Ferroelectric Transistors," in *2022 International Electron Devices Meeting (IEDM)*, 3-7 Dec. 2022, pp. 11.1.1-11.1.4.

[4] C. Liu, Wang, W. Yang, T. Cao, L. Chen, M. Li, F. Liu, D. K. Loke, J. Kang, and Y. Zhu, "Multiscale Modeling of $Al_{0.7}Sc_{0.3}N$-based FeRAM: the Steep Switching, Leakage and Selector-free Array," in *2021 IEEE International Electron Devices Meeting (IEDM)*, 11-16 Dec. 2021, pp. 8.1.1-8.1.4.

[5] J. Casamento, H. Lee, C. S. Chang, M. F. Besser, T. Maeda, D. A. Muller, H. Xing, and D. Jena, "Strong effect of scandium source purity on chemical and electronic properties of epitaxial ScxAl1−xN/GaN heterostructures," *APL Materials,* vol. 9, no. 9, p. 091106, 2021.

[6] D. Wang, P. Wang, S. Mondal, Y. Xiao, M. Hu, and Z. Mi, "Impact of dislocation density on the ferroelectric properties of ScAlN grown by molecular beam epitaxy," *Applied Physics Letters,* vol. 121, no. 4, p. 042108, 2022.

[7] S. Satoh, K. Ohtaka, T. Shimatsu, and S. Tanaka, "Crystal structure deformation and phase transition of AlScN thin films in whole Sc concentration range," *Journal of Applied Physics,* vol. 132, no. 2, p. 025103, 2022.

[8] K. Furuta, K. Hirata, S. A. Anggraini, M. Akiyama, M. Uehara, and H. Yamada, "First-principles calculations of spontaneous polarization in ScAlN," *Journal of Applied Physics,* vol. 130, no. 2, p. 024104, 2021.

[9] A. R. Oganov and C. W. Glass, "Crystal structure prediction using ab initio evolutionary techniques: Principles and applications," *The Journal of Chemical Physics,* vol. 124, no. 24, p. 244704, 2006.

[10] A. R. Oganov, A. O. Lyakhov, and M. Valle, "How Evolutionary Crystal Structure Prediction Works—and Why," Accounts of Chemical Research, vol. 44, no. 3, pp. 227-237, 2011.

[11] A. O. Lyakhov, A. R. Oganov, H. T. Stokes, and Q. Zhu, "New developments in evolutionary structure prediction algorithm USPEX," *Computer Physics Communications,* vol. 184, no. 4, pp. 1172-1182, 2013.

[12] A. Zunger, S.-H. Wei, L. Ferreira, and J. E. Bernard, "Special quasirandom structures," *Physical Review Letters,* vol. 65, no. 3, p. 353, 1990.

[13] J. P. Perdew, K. Burke, and M. Ernzerhof, "Generalized Gradient Approximation Made Simple," *Physical Review Letters,* vol. 77, no. 18, pp. 3865-3868, 1996.

[14] P. E. Blöchl, "Projector augmented-wave method," *Physical Review B,* vol. 50, no. 24, pp. 17953-17979, 1994.

[15] G. Kresse and D. Joubert, "From ultrasoft pseudopotentials to the projector augmented-wave method," *Physical Review B,* vol. 59, no. 3, pp. 1758-1775, 1999.

[16] G. Kresse and J. Furthmüller, "Efficient iterative schemes for ab initio total-energy calculations using a plane-wave basis set," *Physical Review B,* vol. 54, no. 16, pp. 11169-11186, 1996.

[17] R. Resta, "Macroscopic polarization in crystalline dielectrics: the geometric phase approach," *Reviews of Modern Physics,* vol. 66, no. 3, pp. 899-915, 1994.

[18] R. D. King-Smith and D. Vanderbilt, "Theory of polarization of crystalline solids," *Physical Review B,* vol. 47, no. 3, pp. 1651-1654, 1993.

[19] C. E. Dreyer, A. Janotti, C. G. Van de Walle, and D. Vanderbilt, "Correct Implementation of Polarization Constants in Wurtzite Materials and Impact on III-Nitrides," *Physical Review X,* vol. 6, no. 2, p. 021038, 2016.

[20] D. Sheppard, P. Xiao, W. Chemelewski, D. D. Johnson, and G. Henkelman, "A generalized solid-state nudged elastic band method," *The Journal of Chemical Physics,* vol. 136, no. 7, p. 074103, 2012.

[21] L. Lodeiro and T. Rauch, "DensityTool: A post-processing tool for space- and spin-resolved density of states from VASP," *Computer Physics Communications,* vol. 277, p. 108384, 2022.

[22] K. Momma and F. Izumi, "VESTA 3 for three-dimensional visualization of crystal, volumetric and morphology data," *Journal of Applied Crystallography,* vol. 44, no. 6, pp. 1272-1276, 2011.